Comparing the performance of OFDM and FBMC multicarrier systems in doubly-dispersive wireless channels

Davide Mattera, Mario Tanda, Maurice Bellanger

▶ **To cite this version:**

Davide Mattera, Mario Tanda, Maurice Bellanger. Comparing the performance of OFDM and FBMC multicarrier systems in doubly-dispersive wireless channels. Signal Processing, 2021, 179, pp.107818. 10.1016/j.sigpro.2020.107818 . hal-03026110

HAL Id: hal-03026110
https://hal.science/hal-03026110

Submitted on 26 Nov 2020

HAL is a multi-disciplinary open access archive for the deposit and dissemination of scientific research documents, whether they are published or not. The documents may come from teaching and research institutions in France or abroad, or from public or private research centers.

L'archive ouverte pluridisciplinaire **HAL**, est destinée au dépôt et à la diffusion de documents scientifiques de niveau recherche, publiés ou non, émanant des établissements d'enseignement et de recherche français ou étrangers, des laboratoires publics ou privés.

Distributed under a Creative Commons Attribution - NonCommercial 4.0 International License

Comparing the performance of OFDM and FBMC multicarrier systems in doubly-dispersive wireless channels

Davide Mattera[a], Mario Tanda[a,*], Maurice Bellanger[b]

[a]*Dipartimento di Ingegneria Elettrica e delle Tecnologie dell'Informazione, Università degli Studi di Napoli Federico II, via Claudio 21, I-80125 Napoli, Italy.*
[b]*CNAM-Electronique, 292 rue Saint-Martin, 75141 Paris cedex 03, France.*

Abstract

In mobile communications, the most widely used multicarrier technique, namely OFDM, is known to exhibit performance limitations in high speed scenarios. FBMC is an alternative approach and, among FBMC techniques, the recently introduced FBMC-PAM scheme has emerged as the most robust to CFO. Therefore, it is chosen here as the challenger of OFDM for performance comparison in doubly dispersive channels. After presentation of the system model, multicarrier scheme and wireless channel, an analytical evaluation of the BER in the particular case of single path time-varying channel is provided for FBMC-PAM and validated through simulations. Then, simulation results are reported for both OFDM and FBMC-PAM, using the 3GPP multipath channel models. It appears that FBMC-PAM can outperform OFDM in highly time-varying frequency-selective channels.

Keywords: FBMC, OFDM, PAM, doubly dispersive channel

*Corresponding author. Tel. +39-081-768-3791. Fax +39-081-768-5925.
Email addresses: mattera@unina.it (Davide Mattera), tanda@unina.it (Mario Tanda), bellang@cnam.fr (Maurice Bellanger)

1. Introduction

Filter bank multicarrier (FBMC) techniques are potential alternatives to the current orthogonal frequency division multiplexing (OFDM) schemes for some emerging applications fields such as machine type communications (MTC) or cognitive radio [1]. In these systems the prototype filter controls performance and a number of operational aspects. Long filters assure high of out-of-band attenuation and asynchronous user coexistence. The performance of offset-quadrature amplitude modulation (OQAM) combined with the isotropic orthogonal transform algorithm prototype filter with overlapping factor K= $4, 6$, in terms of mean-square error, has been analyzed through computer simulations in [2].

However, for reduced system latency or robustness to time-varying channels, short prototype filters are required. In [3, 4] short prototype filters with overlapping factor K= 2 (i.e., only 2 adjacent multicarrier symbols overlap in time), have been proposed. Since FBMC-OQAM combined with short filters achieves limited performance, the exploitation of the complex lapped transform for transceiver design has been used for the design of the FBMC-PAM transceiver[5–7]. For a special choice of the prototype filter it is much similar to the first analog multicarrier system introduced by Chang [8], whose relation with OFDM/OQAM (for a proper adjustment of the intercarrier spacing) is reported in [9]. An unified view of the two systems by considering the "even-spaced" and "odd-spaced" cases (even or odd multiples of half the subcarrier spacing) is reported in [10].) The scheme is based on pulse amplitude modulation (PAM) combined with a sine prototype filter with overlapping factor K=2 and it achieves full orthogonality, like OFDM. Moreover, the sine prototype filter exhibits a key characteristic, the width of its main lobe in the frequency domain is 3 times the sub-carrier spacing while it is only 2 times for OFDM scheme. The consequence of this enlarged main lobe and of its better spectral decay is that FBMC-PAM outperforms OFDM systems

in terms of CFO sensitivity [11]. However, for mobile communication systems, particularly in high speed condition, sensitivity to doubly-dispersive channels is a key issue that modern multicarrier systems have to face.

This paper deals with the performance analysis of FBMC-PAM and OFDM, in wireless dispersive channels. In particular, it is shown through computer simulations, that in doubly-dispersive channels FBMC-PAM is less sensitive than OFDM to the frequency dispersion. Moreover, the bit error rate (BER) of FBMC-PAM in single-path time-varying channel is analytically evaluated and compared with computer simulation results.

The organization of the paper is as follows. In Section 2, the standard FBMC-PAM system is recalled while in Section 3 the analytical expression of its BER in single-path time-varying channel is derived. Numerical and simulation results are reported in Section 4, and conclusions are drawn in the final Section.

Notation: $j \triangleq \sqrt{-1}$, superscript $(\cdot)^*$ denotes the complex conjugation, $\Re[\cdot]$ the real part, $\Im[\cdot]$ the imaginary part, $\delta[k]$ the Kronecker delta, $|\cdot|$ the absolute value, and $E[\cdot]$ denotes statistical expectation.

2. System Model

Let us consider an FBMC-PAM system [5] with $2M$ subcarriers. The received signal in doubly-dispersive channel can be written as

$$r(t) = \sum_{p=0}^{L-1} g_p(t) s(t - \tau_p) + n(t) \tag{1}$$

where $s(t)$ is the transmitted FBMC-PAM signal, $n(t)$ denotes the zero-mean circular complex white Gaussian noise with independent real and imaginary part, each with two sided power spectral density N_o, and τ_p is the delay of the pth path $g_p(t)$ of the time-varying multipath channel. In (1) each multipath component is modeled as a complex Gaussian process and the different paths of the channel are

assumed to be statistically independent of one another. Moreover, the autocorrelation of the $p-th$ multipath component is

$$E[g_p(t)g_p^*(t-\tau)] = P_g(p)\, J_0(2\pi f_D \tau) \tag{2}$$

where $P_g(p)$ is the power of the random process $g_p(t)$, $J_0(\cdot)$ is the zero-order Bessel function of first kind and f_D is the maximum Doppler shift. The FBMC-PAM signal $s(t)$ is equal to

$$s(t) = \sum_{i=0}^{N_s-1} \sum_{k=0}^{2M-1} d_k[i] e^{j\frac{\pi}{T}\left(k+\frac{1}{2}\right)\left(t-iT+\frac{T}{2}\right)} h(t-iT) \tag{3}$$

where $2T$ is the FBMC-PAM symbol duration, N_s is the number of payload symbols, $d_k[i]$ is the real information symbol transmitted on the kth subcarrier in the ith symbol interval, and $h(t)$ is the real pulse-shaping filter. The mean-square value of the data symbols is denoted as $E[(d_k[i])^2] = P_d$. In the following we assume that the received signal $r(t)$ is filtered with an ideal low-pass filter with a bandwidth of $1/T_s$, where T_s denotes the sampling period. Note that the FBMC-PAM symbol duration is equal to $2T = 2MT_s$.

The discrete-time low-pass version of the received signal can be written as

$$r[l] = \sum_{i=0}^{N_s-1} \sum_{k=0}^{2M-1} \sum_{p=0}^{L-1} g_p[i] d_k[i] T_c[k, l-\theta_p - iM] + v[l] \tag{4}$$

where

$$T_c[k,l] \triangleq h[l]\, e^{j\frac{\pi}{M}\left(k+\frac{1}{2}\right)\left(l+\frac{1}{2}+\frac{M}{2}\right)}, \tag{5}$$

$\theta_p = \tau_p/T_s$ is the normalized delay of the pth path $g_p[i]$ of the time-varying multipath channel assumed to be static over an interval of length M, and $v[l]$ is a discrete-time zero-mean AWGN process with autocorrelation function

$$R_v[m] = E\{v[l]v^*[l-m]\} = \frac{2N_o}{T_s}\delta[m] = \sigma_v^2 \delta[m]. \tag{6}$$

In (5) the real prototype filter $h[l]$, equal to zero for $l \notin \mathcal{K}_{2M} \triangleq \{0, 1, \ldots, 2M-1\}$ and with energy

$$\mathcal{E}_h \triangleq \sum_{l=0}^{2M-1} h^2[l], \tag{7}$$

satisfies the following conditions

$$h[M+l] = h[M-l-1] \qquad \forall\ l, \tag{8}$$

$$\sum_{m=-\infty}^{+\infty} h[l+mM]h[l+mM+2rM] = \delta[r] \qquad \forall\ l, r. \tag{9}$$

that imply the orthogonality condition

$$\frac{1}{M}\Re\left\{\sum_{l=0}^{2M-1} T_c[k,l]T_c^*[m,l-pM]\right\} = \delta[m-k]\delta[p]. \tag{10}$$

In this case, it follows that [5] in AWGN channel the optimum (in the maximum likelihood sense) decision variable for estimating statistically independent information symbols can be written as

$$\hat{d}_m[i] \triangleq \frac{1}{M}\Re\left\{\sum_{l=0}^{2M-1} r[iM+l]T_c^*[m,l]\right\} \tag{11}$$

since conditions (8) and (9) assure the absence of intersymbol interference and intercarrier interference.

In the following it is considered the prototype filter

$$h[l] = \sin\left[\frac{\pi}{2M}\left(l+\frac{1}{2}\right)\right] \quad l \in \mathcal{K}_{2M}, \qquad h[l] = 0 \quad l \notin \mathcal{K}_{2M}. \tag{12}$$

This prototype filter satisfies conditions (8) and (9) and simplifies the receiver as shown in [5]. The magnitude of the Fourier transform of the prototype filter in (12) and of the prototype filter for OFDM is reported in Fig.1 in the case where the length of the two prototype filters is the same, that is, in the case where both systems have the same subcarrier spacing. The figure shows that the prototype filter in (12) assures a better spectral decay and, moreover, its main lobe in the frequency domain is 3 times the sub-carrier spacing instead of 2 times for OFDM.

3. BER evaluation

The BER of OFDM in doubly-selective channels has been evaluated in [12]. In this section we evaluate the BER of FBMC-PAM in the particular case of single-path time-varying channel.

In a single-path time-varying channel the FBMC-PAM received signal can be written as

$$r[l] = \sum_{i=0}^{N_s-1} \sum_{k=0}^{2M-1} g[i] d_k[i] T_c[k, l - iM] + v[l] \tag{13}$$

where the fading process $g[i]$ has autocorrelation function

$$R_g[m] = E\left\{g[i] g^*[i-m]\right\}. \tag{14}$$

The considered receiver is based on (11) thus, omitting the irrelevant factor $\frac{1}{M}$ and taking into account (4), we can write

$$\begin{aligned} &\Re\left\{\sum_{l=0}^{2M-1} r[iM+l] T_c^*[m,l]\right\} \\ &= \Re\left\{\left[\sum_{q=i-1}^{i+1} \sum_{k=0}^{2M-1} d_k[q] \sum_{\zeta=0}^{1} \sum_{l=0}^{M-1} g[i+\zeta] T_c[k, l+(i+\zeta-q)M]\right] T_c^*[m, l+\zeta M] \right. \\ &\qquad \left. + \sum_{l=0}^{2M-1} v[iM+l] T_c^*[m,l]\right\}. \end{aligned} \tag{15}$$

where the sum over ζ takes into account the length $2M$ of the prototype filter (see (5) and (12)). After simple manipulations we obtain

$$\Re\left\{\sum_{l=0}^{2M-1} r[iM+l] T_c^*[m,l]\right\} = \Re\left\{d_m[i]\alpha + \beta + \gamma + \delta\right\} \tag{16}$$

where

$$\alpha \triangleq \sum_{\zeta=0}^{1} g[i+\zeta] \sum_{l=0}^{M-1} h^2[l+\zeta M], \tag{17}$$

$$\beta \triangleq \sum_{k=0, k\neq m}^{2M-1} d_k[i] \sum_{\zeta=0}^{1} g[i+\zeta] \sum_{l=0}^{M-1} T_c[k, l+\zeta M] T_c^*[m, l+\zeta M], \tag{18}$$

$$\gamma \triangleq \sum_{n=-1,n\neq 0}^{1} \sum_{k=0}^{2M-1} d_k[i+n] \sum_{\zeta=0}^{1} g[i+\zeta] \sum_{l=0}^{M-1} T_c[k, l+(\zeta-n)M] T_c^*[m, l+\zeta M], \quad (19)$$

and

$$\delta \triangleq \sum_{l=0}^{2M-1} v[iM+l] T_c^*[m,l]. \quad (20)$$

It is assumed that the receiver has perfect knowledge of the term α in (17) that multiplies the datum of interest $d_m[i]$, and then we can write

$$\hat{d}_m[i] = \frac{d_m[i]}{\sqrt{P_d}} + I_m[i] \quad (21)$$

where the disturbance term $I_m[i]$ is defined as

$$I_m[i] \triangleq \Re\left\{\frac{\beta+\gamma+\delta}{\alpha\sqrt{P_d}}\right\}. \quad (22)$$

Note that the disturbance $I_m[i]$ depends on the data transmitted in the ith multicarrier symbol on the subcarriers with index $k \neq m$ (inter-carrier interference (ICI)) and on the data transmitted adjacent multicarrier symbols with indices $i-1$ and $i+1$ (inter-symbol interference (ISI)). Let us denote a particular (interfering) data symbol combination as $z_m^d[i]$. The PDF of the disturbance $I_m[i]$ conditioned upon a particular data symbol combination $z_m^d[i]$, denoted as $f_{I_m[i]|d}(x \mid d)$, is the PDF of the real part of the ratio between two correlated complex Gaussian random variables and can be determined by exploiting the following theorem derived in [13]: if U and V are zero-mean correlated complex Gaussian random variables with variance $\sigma_U^2 = E[|\ U\ |^2]$ and $\sigma_V^2 = E[|\ V\ |^2]$, respectively, and correlation coefficient $\rho = \rho_r + j\rho_i = \frac{E[U^*V]}{\sigma_U\sigma_V}$, the PDF of the random variable $Z_r = \Re\left\{\frac{U}{V}\right\}$ is given by

$$f_{Z_r}(x) = \frac{1}{2}\frac{\sigma_U^2}{\sigma_V^2} \frac{1-\rho_r^2-\rho_i^2}{\left[(1-\rho_i^2)\frac{\sigma_U^2}{\sigma_V^2} - 2\rho_r\frac{\sigma_U}{\sigma_V}x + x^2\right]^{\frac{3}{2}}}. \quad (23)$$

Note that the expression in (23) has been derived by performing some simple manipulations on (13) in [14] that has been obtained by taking the derivative of (18) in [13].

It can be shown that for a particular data symbol combination $z_m^d[i]$

$$\frac{\sigma_U^2}{\sigma_V^2} = \frac{\mid A[0] \mid^2 + \mid A[1] \mid^2 + 2\rho_g \Re\{A[0]A^*[1]\} + \frac{1}{SNR}}{\frac{1}{2}(1+\rho_g)} \tag{24}$$

and

$$\rho = \frac{(1+\rho_g)(A^*[0] + A^*[1])}{\sqrt{\left[\mid A[0] \mid^2 + \mid A[1] \mid^2 + 2\rho_g \Re\{A[0]A^*[1]\} + \frac{1}{SNR}\right] 2(1+\rho_g)}} \tag{25}$$

where for $\zeta = 0, 1$

$$A[\zeta] \triangleq \frac{1}{\mathcal{E}_h \sqrt{P_d}} \left\{ \sum_{k=0, k\neq m}^{2M-1} d_k[i] \sum_{l=0}^{M-1} T_c[k, l+\zeta M] T_c^*[m, l+\zeta M] \right.$$

$$\left. + \sum_{n=-1, n\neq 0}^{1} \sum_{k=0}^{2M-1} d_k[i+n] \sum_{l=0}^{M-1} T_c[k, l+(p-n)M] T_c^*[m, l+pM] \right\}, \tag{26}$$

$$\rho_g \triangleq \frac{R_g[1]}{R_g[0]} \tag{27}$$

is the channel fading correlation coefficient and

$$SNR \triangleq \frac{P_d \mathcal{E}_h R_g[0]}{\sigma_v^2}. \tag{28}$$

Note that the signal-to-noise ratio in (28) is equal to E_s/N_o that is the ratio between the energy of the real radio-frequency signal, in each multicarrier symbol interval of duration $T = MT_s$ and for each active subcarrier, divided by spectral density level N_o. For a particular (interfering) data symbol combination $z_m^d[i]$ the conditional PDF of the disturbance $f_{I_m[i]|d}(x \mid d)$ can be evaluated by using (23) and (24) - (28). Therefore, the unconditional PDF of the disturbance $f_{I_m[i]}(x)$ can be evaluated by averaging over the different data symbols combinations $z_m^d[i]$. Once the PDF of the disturbance $f_{I_m[i]}(x)$ has been obtained, the BER can be evaluated by taking into account the considered PAM system.

Note that the previous approach can be exploited also to take into account the presence of a carrier frequency offset (CFO) in the receiver. In particular, in this

case the received signal can be written as

$$r[l] = \sum_{i=0}^{N_s-1} \sum_{k=0}^{2M-1} g[i] d_k[i] T_c[k, l - iM] e^{j\frac{2\pi}{2M}\epsilon l} + v[l] \tag{29}$$

where $\epsilon = \Delta f 2T$ is the CFO (Δf) normalized to the subcarrier spacing $1/(2T)$. For a particular (interfering) data symbol combination $z_m^d[i]$ and a fixed value of the CFO ϵ the conditional PDF of the disturbance $f_{I_m[i],\epsilon|d}(x \mid d)$ is obtained by exploiting the PDF

$$f_{Z_r,\epsilon}(x) = \frac{1}{2} \frac{\sigma_U^2(\epsilon)}{\sigma_V^2(\epsilon)} \frac{1 - \rho_r^2(\epsilon) - \rho_i^2(\epsilon)}{\left[(1 - \rho_i^2(\epsilon)) \frac{\sigma_U^2(\epsilon)}{\sigma_V^2(\epsilon)} - 2\rho_r(\epsilon) \frac{\sigma_U(\epsilon)}{\sigma_V(\epsilon)} x + x^2 \right]^{\frac{3}{2}}} \tag{30}$$

where

$$\frac{\sigma_U^2(\epsilon)}{\sigma_V^2(\epsilon)} = \frac{W}{\mid G[0,\epsilon] \mid^2 + \mid G[1,\epsilon] \mid^2 + 2\rho_g \Re \{G[0,\epsilon] G^*[1,\epsilon]\}} \tag{31}$$

and

$$\rho(\epsilon) = \frac{A^*[0,\epsilon] G[0,\epsilon] + A^*[1] G[1,\epsilon] + \rho_g \{A^*[0,\epsilon] G[1,\epsilon] + A^*[1,\epsilon] G[0,\epsilon]\}}{\sqrt{W \left[\mid G[0,\epsilon] \mid^2 + \mid G[1,\epsilon] \mid^2 + 2\rho_g \Re \{G[0,\epsilon] G^*[1,\epsilon]\} \right]}} \tag{32}$$

with

$$W \triangleq \mid A[0,\epsilon] \mid^2 + \mid A[1,\epsilon] \mid^2 + 2\rho_g \Re \{A[0,\epsilon] A^*[1,\epsilon]\} + \frac{1}{SNR}. \tag{33}$$

Moreover, in (31), (32), and (33), for $\zeta = 0, 1$,

$$A[\zeta,\epsilon] \triangleq \frac{1}{\mathcal{E}_h \sqrt{P_d}} \left\{ \sum_{k=0, k\neq m}^{2M-1} d_k[i] \sum_{l=0}^{M-1} T_c[k, l + \zeta M] T_c^*[m, l + \zeta M] e^{j\frac{2\pi}{2M}\epsilon(l+\zeta M)} \right.$$

$$\left. + \sum_{n=-1, n\neq 0}^{1} \sum_{k=0}^{2M-1} d_k[i+n] \sum_{l=0}^{M-1} T_c[k, l + (\zeta - n)M] T_c^*[m, l + \zeta M] e^{j\frac{2\pi}{2M}\epsilon(l+\zeta M)} \right\} \tag{34}$$

and

$$G[\zeta,\epsilon] \triangleq \frac{1}{\mathcal{E}_h} \sum_{l=0}^{M-1} h^2[l + \zeta M] e^{j\frac{2\pi}{2M}\epsilon(l+\zeta M)}. \tag{35}$$

Once for a particular (interfering) data symbol combination $z_m^d[i]$ the conditional PDF of the disturbance $f_{I_m[i],\epsilon|d}(x \mid d)$ has been evaluated by using (30) and

(31) - (35), the unconditional PDF of the disturbance $f_{I_m[i],\epsilon}(x)$ can be obtained by averaging over the different data symbols combinations $z_m^d[i]$.

4. Simulation results

In this section, at first simulations results in time-varying single-path channel are presented and compared with the previously derived BER analytical expression for FBMC-PAM. Then, the BER performance of the FBMC-PAM system in doubly-selective channel is assessed via computer simulations and compared with that of the OFDM system.

4.1. Simulation results in time-varying single-path channel

The simulation results in time-varying single-path channel are obtained under the following conditions.

1. The channel fading is modeled as a lightly damped second-order autoregressive (AR) process

$$g[i] = -\beta_1 g[i-1] - \beta_2 g[i-2] + n_g[i] \tag{36}$$

where $g[i]$ is the channel fading coefficient in the ith symbol interval, the noise process $n_g[i]$ is a zero-mean complex white Gaussian process, and the AR parameters β_1 and β_2 are related to the physical parameters of the fading channel [15]. In particular,

$$\beta_1 = -2r_d \cos(2\pi f_p T) \tag{37}$$

and

$$\beta_2 = r_d^2 \tag{38}$$

where f_p is the spectral peak frequency, T is the multicarrier symbol interval, and r_d is the pole radius. It was stated in [16] and justified in [17] that

when $f_p = f_D/\sqrt{(2)}$ (f_D is the maximum Doppler shift in (2)), the autocorrelation function of the AR process in (36) is close, for moderate values of m, to that of the Jakes model in (2). The pole radius and the carrier frequency have been fixed at $r_d = 0.998$ and $f_0 = 2GHz$, respectively. (Note that the knowledge of the carrier frequency allows one to easily find the relationship between the mobile speed reported in the figures in the following and the maximum Doppler shift f_D reported in (2)).

2. The total number of subcarriers for both the considered systems is $2M = 128$, and, the transmitted data belong to a 2-PAM constellation in the FBMC-case and to a 4-QAM constellation in the OFDM case. The total bandwidth of both systems is B =2.5 MHz.
3. The BER values are obtained by averaging over bursts of 10 payload symbols received in 10^4 independent channel realizations.

Figure 2 shows the BER of 2-PAM (FBMC) versus E_b/N_o in single-path fading channel, solid curves and marks denote the analytical and the simulation results, respectively. The results show that the analytical expressions derived in previous section can be exploited to predict accurately the actual BER of the system. In particular, as one would expect, as the moving speed increases a performance degradation is observed and a floor appears for high E_b/N_o values. The gap between the performance at 5 km/h and 500 km/h increases as E_b/N_o increases, however, it is quite contained for $E_b/N_o \leq 25$dB.

Figure 3 shows the BER obtained by computer simulations of 2-PAM (FBMC) and 4-QAM (OFDM) versus E_b/N_o in time-selective single-path fading channel. The results show that FBMC-PAM and OFDM systems achieve similar performance in the considered single-path time-varying fading channel. Note that, although the sine prototype filter of FBMC-PAM has better spectral characteristics than the rectangular prototype filter of OFDM, in the considered scenario the one-

tap equalizer in FBMC-PAM case operates in the presence of both ICI and ISI while in the OFDM case only ICI is present.

Figure 4 shows the BER obtained by computer simulations (solid lines) of 2-PAM (FBMC) and 4-QAM (OFDM) versus the normalized CFO ϵ in the time-selective single-path fading channel (29) for $E_b/N_o = 30$dB and two values of the moving speed (5 km/h and 100 km/h). Moreover, the BER of 2-PAM (FBMC) obtained by exploiting analytical results (dashed lines) is also reported. The results show that the analytical expressions derived in the previous section can be exploited to predict accurately the actual BER of the FBMC-PAM system also in the presence of a CFO. In the considered scenario it is evident the robustness of the FBMC-PAM system to the CFO while the OFDM system presents a severe performance degradation as the CFO increases.

4.2. Simulation results in doubly-selective channel

The simulation results in doubly-selective channel are obtained under the following conditions.

1. Each multipath channel fading component $g_p[i]$ is modeled as in (36), (37) and (38).
2. The total number of subcarriers for the considered FBMC-PAM system is $2M = 1024$, and, the transmitted data belong to a 2-PAM or a 8-PAM constellation. Moreover, the total number of subcarriers for the considered OFDM system is $M^{OFDM} = 1024$ and the transmitted data belong to a 4-QAM or a 64-QAM constellation. Note that in this case both systems have the same subcarrier spacing, and, moreover, the same bit rate (when the number of active subcarriers is the same for both systems and in the absence of the cyclic prefix (CP)) since the symbol rate of FBMC, whose overlapping factor is $K = 2$, is twice that of OFDM. In the following experiments the actual bit rate of FBMC is slightly larger than that of OFDM since

the FBMC system has 912 active subcarriers while the OFDM system has 840 active subcarriers, and, moreover, the CP of OFDM is different from zero.

3. The considered multipath channel model Extended Pedestrian A (EPA) [18] has the following power/delay profile: relative power (in dB) equal to [0 −1 −2 −3 −8 −17.2 −20.8] and delay (in discrete samples) [0 1 2 3 4 5 8]. Moreover, the considered Extended Vehicular A (EVA) [18] multipath channel model has the following power/delay profile: relative power (in dB) equal to [0 −1.5 −1.4 −3.6 −0.6 −9.1 −7 −12 −16.9] and delay (in discrete samples) [0 1 3 6 7 14 22 35 50]. Finally, the considered multipath channel model Extended Typical Urban (ETU) [18] has the following power/delay profile: relative power (expressed in dB) equal to [−1 −1 −1 0 0 0 −3 −5 −7] and delay (expressed in discrete samples) equal to [0 1 2 4 5 10 32 46 100].
4. The BER values are obtained by averaging over bursts of 10 payload symbols received in 10^3 independent channel realizations.

Figure 5 shows the BER of 2-PAM (FBMC) and 4-QAM (OFDM) versus E_b/N_o in static and in doubly-selective EPA channel. The results show the performance degradation of the receiver for both systems due to the frequency-domain dispersion related to the time-variability of the channel. In particular, while the performance of both systems in the static channel case is practically coincident, the OFDM system presents a more severe performance degradation when the moving speed increases.

Figure 6 shows the BER of both systems as a function of the moving speed for two different values of E_b/N_o and in the absence of noise (see the curves labeled as $E_b/N_o = inf$). Of course in this last case the performance degradation is due only to the loss of orthogonality among the subcarriers in the considered frequency-

dispersive channel. The results show that, for $E_b/N_o = 30$dB, the FBMC-PAM system outperforms the OFDM system for a moving speed larger than 100 km/h. Note that, in the absence of noise and in the static channel, the FBMC-PAM system presents a BER value different from zero due to the presence of residual interference while the single-tap equalizer in the OFDM system, due to the presence of the CP, provides only correct decisions (thus, the mark for the OFDM system at moving speed equal to zero is absent). However, also in the absence of noise, as the moving speed increases, FBMC-PAM results to be more robust than OFDM. In particular, the performance cross-over in the absence of noise is at a moving speed slightly larger than 100 km/h.

Figure 7 shows the BER versus E_b/N_o of both systems in static and in doubly-selective EVA channel. As one would expect, in this more time-dispersive (and, then, more frequency-selective) channel a performance degradation of the FBMC-PAM system with respect to the OFDM system is observed for low values of the moving speed, since the presence of the CP in the OFDM system assures (nearly) perfect one-tap channel equalization while the one-tap equalizer in the FBMC-PAM case operates in the presence of residual interference. However, as the speed increases, the performance degradation of the OFDM system is more severe and, for a sufficiently high value of the moving speed, a performance cross-over is observed. This effect is more clearly observed in Figure 8 for some values of E_b/N_o.

Figure 9 shows the BER versus E_b/N_o of both systems in static and in doubly-selective ETU channel. In this highly frequency-selective channel, the performance degradation of the FBMC-PAM system with respect to the OFDM system for moderate and high values of E_b/N_o and for the considered values of the moving speed, is severe. In particular, the curves present a floor at a BER value larger than that assured by the OFDM system also for very high values of the moving

speed. This effect can be clearly observed for some values of E_b/N_o in Figure 10.

Figure 11 shows the BER of 8-PAM (FBMC) and 64-QAM (OFDM) versus E_b/N_o of both systems in static and in doubly-selective EPA channel. The results show that as the moving speed increases the BER of the OFDM system increases more rapidly than that of the FBMC system. In particular, in the considered case, if the moving speed is higher than 100 km/h, the FBMC-PAM system outperforms the OFDM system.

Figure 12 shows the BER of both systems as a function of the moving speed for two different values of E_b/N_o and in the absence of noise. The results show that, for $E_b/N_o = 30$dB, the FBMC-PAM system outperforms the OFDM system nearly in the whole range of the considered moving speeds. Note that also in the absence of noise, as the moving speed increases, the performance degradation of the single-tap equalizer for FBMC-PAM results to be more contained than that observed in the OFDM case. In particular, the performance cross-over point in the absence of noise is at a moving speed of 50 km/h.

Figure 13 shows the BER versus E_b/N_o of both systems in static and in doubly-selective EVA channel. The results show that, as the speed increases, the performance degradation of the OFDM system is more severe and, then, for a sufficiently high value of the moving speed a performance cross-over is observed. This effect is more evident in Figure 14 where it is shown that the FBMC-PAM system outperforms the OFDM system for high values of E_b/N_o at a moving speed greater than 200 km/h. For $E_b/N_o = 20$dB the cross-over point is around 100 km/h, however, the performance degradation of the OFDM system with respect to the FBMC-PAM system is more contained.

A performance behaviour similar to that observed in the previous four figures is present also in Figure 15 that shows the BER versus E_b/N_o of both systems in static and in doubly-selective ETU channel. In this highly frequency-selective

channel the performance degradation of the FBMC-PAM system with respect to the OFDM system, for moderate and high values of E_b/N_o and for low values of the moving speed, is quite severe. However, as the speed increases, the performance of the OFDM system is more sensitive to the channel frequency dispersion and, again, for a sufficiently high value of the moving speed a performance cross-over is observed. This effect can be observed in Figure 16 for some fixed values of E_b/N_o. Note that, in the FBMC-PAM case, the performance at $E_b/N_o = 30$dB is nearly equal to that in the absence of the noise; thus, in this case the residual interference is more relevant than the additive noise.

By comparing the results for 2-PAM (4-QAM) and those for 8-PAM (64-QAM) in the different channels, it follows that the performance cross-over points, when present (see Figures 6 and 12 for EPA channel and Figures 8 and 14 for EVA channel), are observed for lower values of the moving speed in the 8-PAM (64-QAM) case. Moreover, Figures 10 and 16 for ETU channel show that, while in the 2-PAM (4-QAM) case the OFDM system outperforms the FBMC-PAM in the whole range of values of considered moving speeds, in the 8-PAM (64-QAM) case a performance cross-over is observed for very high values of the moving speed.

To gain some insight into the actual performance of both FBMC-PAM and OFDM systems as the relative channel frequency-dispersion increases, in figures 17 and 18 it is reported the BER as a function of M for a fixed value of E_b/N_o and some values of the moving speed. In particular, 8-PAM (FBMC) and 64-QAM (OFDM) constellations are used in figures 17 and 18, respectively.

Note that the performance of the FBMC system in static channel for high values of M achieves a floor at a BER value equal to that in frequency-flat channel since, for a sufficiently large number of subcarriers, the residual interference is negligible. However, for a moderate value of the moving speed, as M increases,

at first a performance improvement is observed, while for higher values of M a degradation is present. Thus, there is an optimum value of M that leads to the minimization of the BER. In the case of the OFDM system (see Fig.18), for a moderate moving speed value and for a low value of M, the channel frequency-dispersion relative to the subcarrier spacing is contained and a performance similar to that in the static channel case is observed. However, as the number of subcarriers increases the subcarrier spacing decreases and the channel frequency-dispersion leads to a severe performance degradation. This effect is observed also for high values of the moving speed; in particular, the higher is the speed, the lower is the number of subcarriers that leads to a BER similar to that observed in static channel.

5. Conclusions

The FBMC-PAM transceiver with its capabilities in terms of spectral efficiency, asynchronous access and protection of adjacent users, has the potential to meet many requirements imposed by the future wireless systems [19, 20].

In this paper, the performance of FBMC-PAM in dispersive channels is analyzed and compared with that of OFDM. In particular, an analytical expression for the BER of FBMC-PAM in single-path time-varying channel that can take into account also the presence of a CFO in the receiver, has been derived. Moreover, simulation results have been exploited to obtain the BER of both systems in single-path time-varying channels and doubly-dispersive wireless channels. In the last case both 2-PAM FBMC/4 QPSK OFDM and 8-PAM FBMC/64-QAM OFDM have been considered.

The results have shown that in single-path time-varying channel both systems assure similar performance in the absence of CFO, while their performance is quite different when a frequency shift is present in addition to the frequency

spread. Specifically, the FBMC-PAM system is quite robust to the frequency shift while the OFDM system presents a severe performance degradation as the CFO increases.

In time-varying and frequency-selective channels, FBMC-PAM results to be less sensitive to frequency dispersion than OFDM and, then, as the mobile velocity increases, a performance cross-over can be observed. For example, for $E_b/N_0 =$ 30dB, in EPA channel with binary signaling (2-PAM FBMC/4-QPSK OFDM) the cross-over is observed at 100 km/h while in EVA channel the cross-over is observed at 200 km/h if 8-PAM (FBMC) and 64-QAM (OFDM) constellations are used. Moreover, for a fixed doubly-dispersive channel model, if the cross-over is present for both the considered symbol constellations, it is observed for lower values of the moving speed in the more spectrally efficient case. Future work will be focused on the derivation of the analytical BER for FBMC-PAM in doubly-dispersive wireless channels and on the sensitivity analysis in the presence of imperfect channel knowledge.

References

References

[1] Y. Medjahdi, S. Traverso, R. Gerzaguet, H. Shaïek. R. Zayani, D. Demmer, R. Zakatia, J.P. Doré, M. Ben Mabrouk, D.Le Ruyet, Y.Louët and D. Roviras, On the road to 5G: comparative study of physical layer in MTC context, IEEE Access. vol. 5, pp. 26556-26581, 2017.

[2] L. Zang, P. Xiao, A. Zafar, A. ul Quddus, R. Tafazolli, FBMC system: an insight into doubly dispersive channel impact, IEEE Trans. on Vehicular Technology, vol. 66, pp. 3942-3956, May 2017.

[3] D. Pinchon, P. Siohan, Derivation of analytical expressions for flexible PR low complexity FBMC systems, Proc. of 21th European Signal Processing Conference (EUSIPCO 2013), pp. 1-5, Sept. 2013.

[4] J. Nadal, C.A. Nour, A. Baghdadi, Design and evaluation of a novel short prototype filter for OFDM/OQAM modulation, IEEE Access. vol. 6, pp. 19610-19625, March 2018.

[5] D. Mattera, M. Tanda, M. Bellanger, Filter bank multicarrier with PAM modulation for future wireless systems, Signal Processing 120 (2016), pp. 594-606.

[6] P. Sabeti, A. Farhang, N. Marchetti and L. Doyle, Performance Analysis of FBMC-PAM in Massive MIMO, 2016 IEEE Globecom Workshops (GC Wkshps), Washington, DC, USA, 2016, pp. 1-7.

[7] C. Sexton, Q. Bodinier, A. Farhang, N. Marchetti, F. Bader, Enabling asynchronous machine-type D2D communication using multiple waveforms in 5G, IEEE Internet of things journal, vol. 5, pp. 1307-1322, April 2018.

[8] R.W. Chang, Synthesis of band-limited orthogonal signals for multichannel data transmission, The Bell System Technical Journal 45 (10) (1966) 1775-1796.

[9] B. Farhang-Boroujeny, Cosine Modulated and offset QAM filter bank multicarrier techniques: A continuous-time prospect, EURASIP Journal on Advances in Signal Processing 2010 (2010) 16.

[10] S. Josilo, M. Pejović, B. Dordević, M. Narandzić, S. Nedić, Multicarrier waveforms with I/Q staggering: uniform and nonuniform FBMC formats, EURASIP Journal on Advances in Signal Processing (2014) (167).

[11] D. Mattera, M. Tanda, M. Bellanger, CFO sensitivity and efficient estimation for the short filter multicarrier system FBMC-PAM, Signal Processing 164 (2019), pp. 10-19.

[12] T.R. Wang, J.G. Proakis, A. Zafar, E. Masry, J.R. Zeidler, Performance degradation of OFDM systems due to Doppler spreading, IEEE Trans. on Wireless Communications, vol. 5, pp. 1422-1432, June 2006.

[13] R.J. Baxley, B.T. Walkenhorst, and G. Acosta-Marum, Complex Gaussian Ratio Distribution with Applications for Error Rate Calculation in Fading Channels with Imperfect CSI, Proc. of 2010 IEEE Global Telecommunications Conference GLOBECOM 2010, Dec. 2010, pp. 1-5.

[14] M. Penner, M. Fuhrwerk, and J. Peissig, Bit Error Probability for Asynchronous Channel Access in Feedback-Less MTC with Scattered Pilot-Based FBMC-OQAM, Proc. of 16th International Symposium on Wireless Communication Systems, ISWCS 2019, pp. 522-526.

[15] P.H. Wu, A. Duel-Hallen, Multiuser detectors with disjoint Kalman channel estimators for synchronous CDMA mobile radio channels, IEEE Trans. Commun. vol. 48, pp. 752-756, May 2000.

[16] L. Lindbom, A Wiener filtering approach to the design of tracking algorithms with applications in mobile radio communications, Ph.D dissertation, Uppsala Univ., Uppsala, Sweden, 1995.

[17] P.H. Wu, A. Duel-Hallen, Multiuser detectors with differentially encoded data for mismatched flat Rayleigh fading channels, Proc. of 30th Annual Conference on Information Sciences and Systems, princeton, NJ, Mar. 1996, pp. 332-337.

[18] 3GPP TS 136 104 version 8.8.0 Release 8, 2010.

[19] M. Shafi et al., 5G: A tutorial overview of standards, trials, challenges, deployment and practice, IEEE JSAC vol. 35, no. 6, June 2017, pp. 1201-1221.

[20] P. Marsh et al., 5G Radio access network architecture: design guidelines and key considerations, IEEE Communications Magazine vol.54, no. 11, Nov. 2016, pp. 24-32.

List of figures

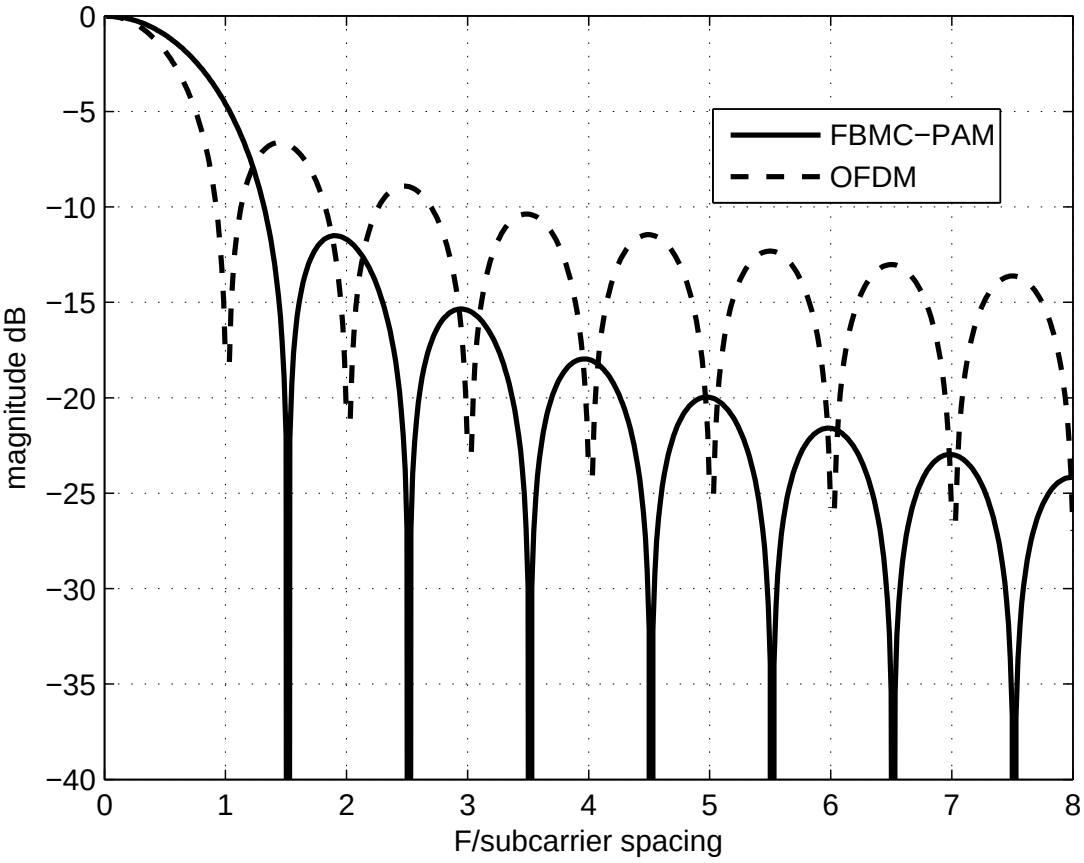

Figure 1: Magnitude of the Fourier transform of the prototype filter of FBMC-PAM and OFDM versus frequency normalized to subcarrier spacing.

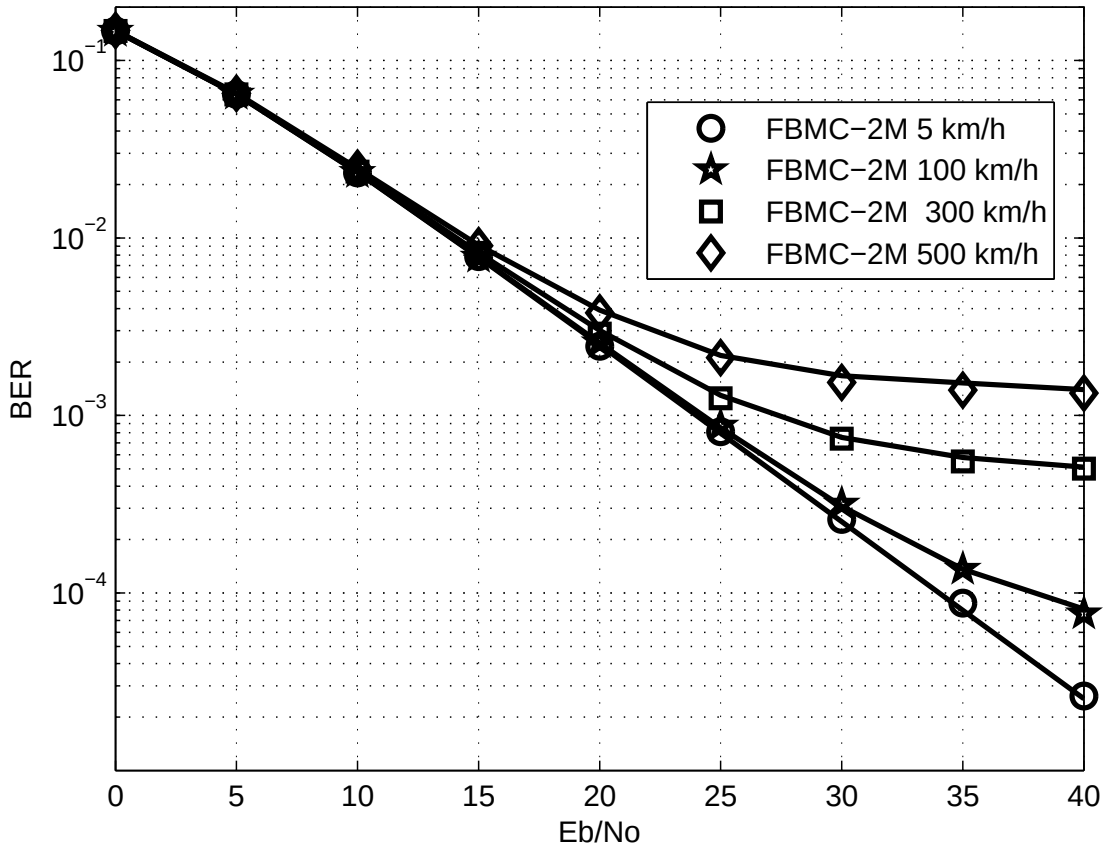

Figure 2: BER of 2-PAM (FBMC) versus Eb/No over single-path time-varying channel, solid lines denote analytical results, marks denote simulation results.

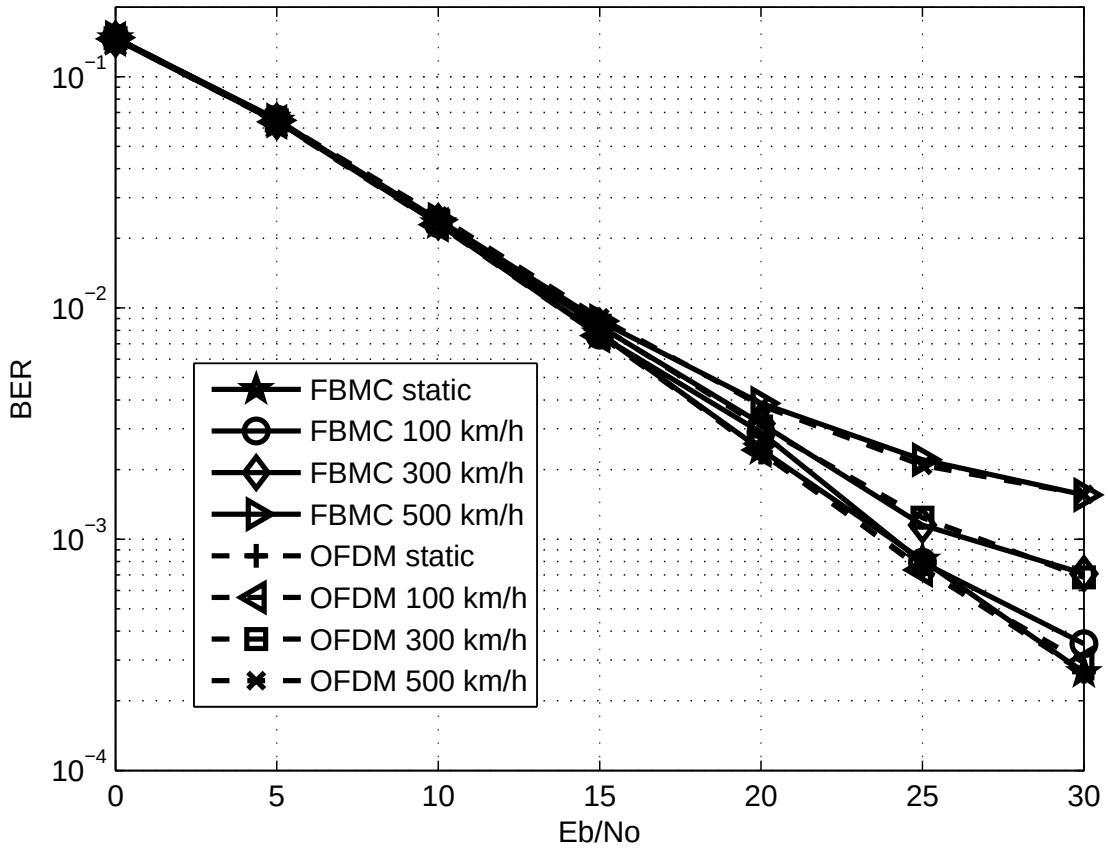

Figure 3: BER of 2-PAM (FBMC) and 4-QAM (OFDM) versus Eb/No over single-path time-varying channel.

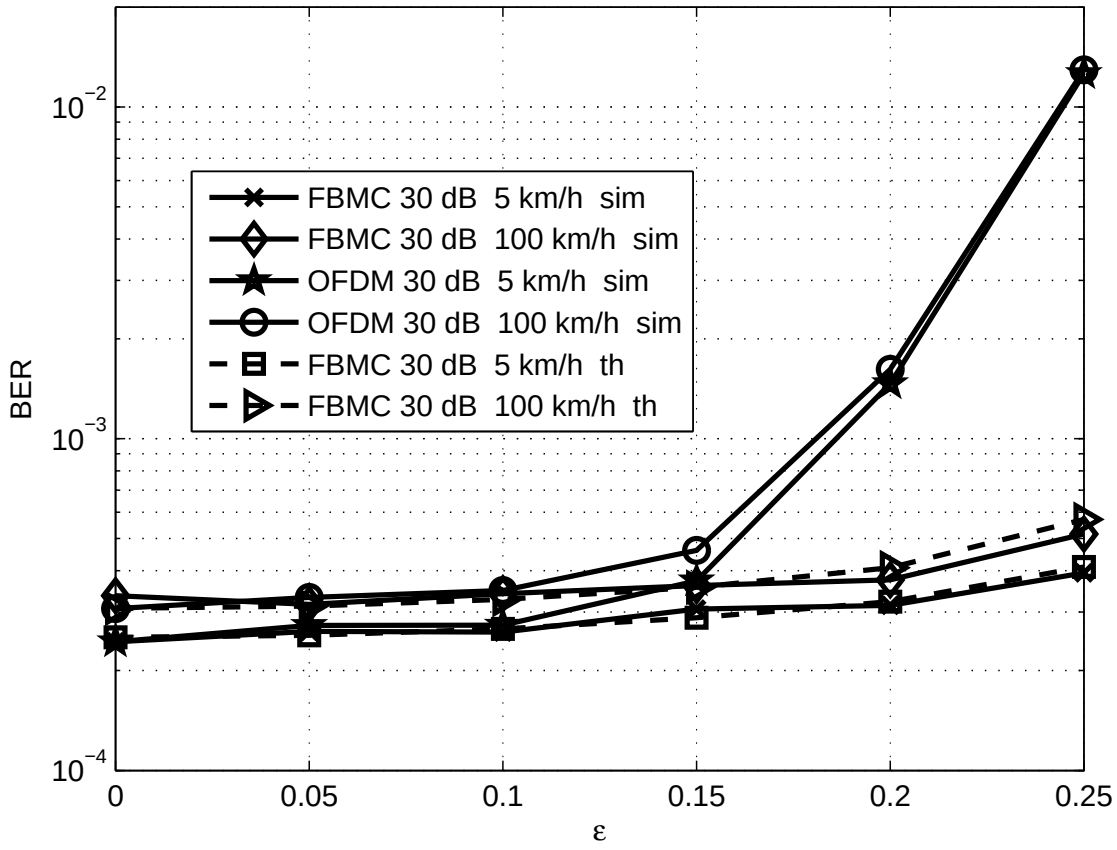

Figure 4: BER of 2-PAM (FBMC) and 4-QAM (OFDM) versus CFO over single-path time-varying channel.

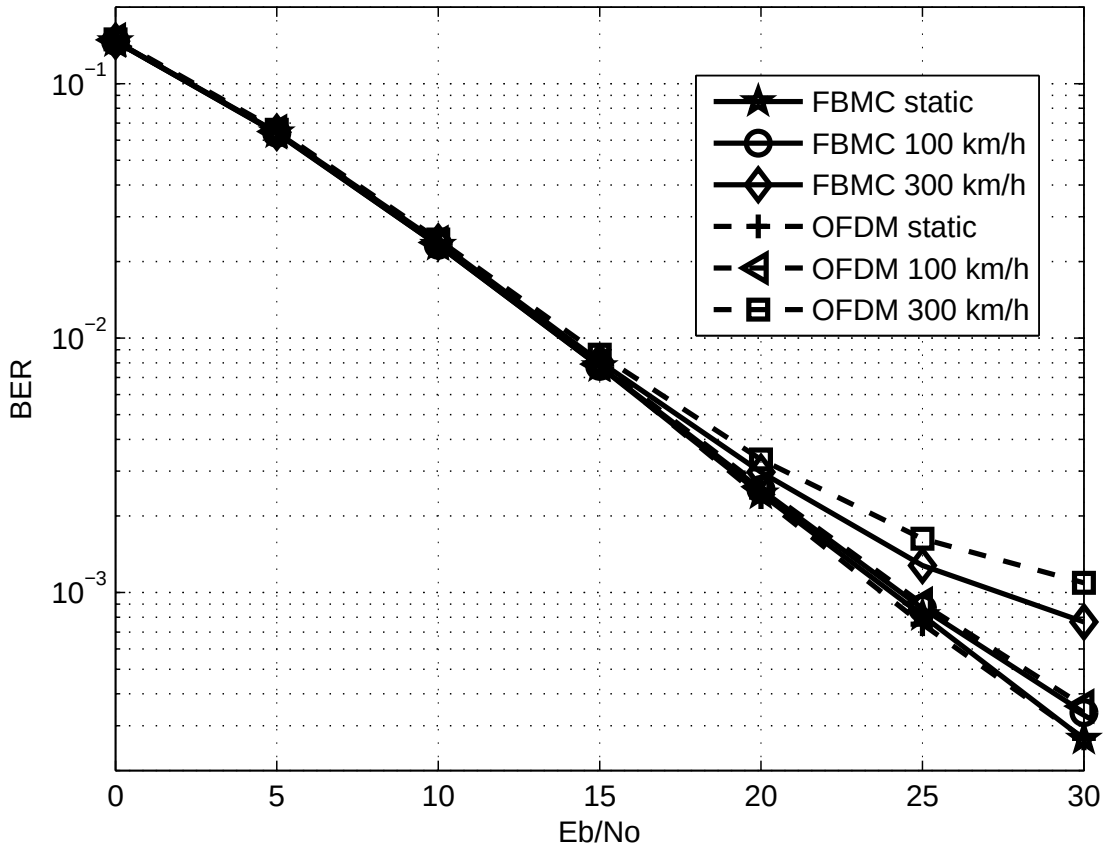

Figure 5: BER of 2-PAM (FBMC) and 4-QAM (OFDM) versus Eb/No over EPA channel.

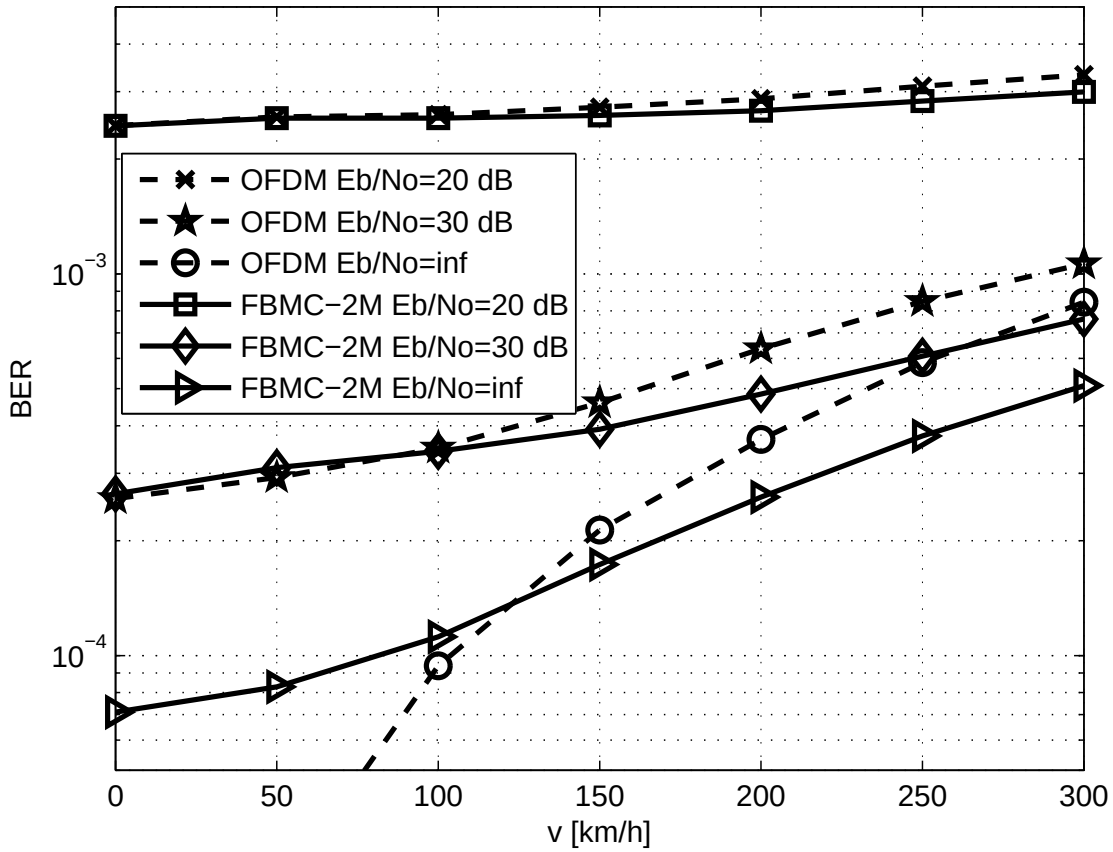

Figure 6: BER of 2-PAM (FBMC) and 4-QAM (OFDM) versus moving speed [km/h] over EPA channel.

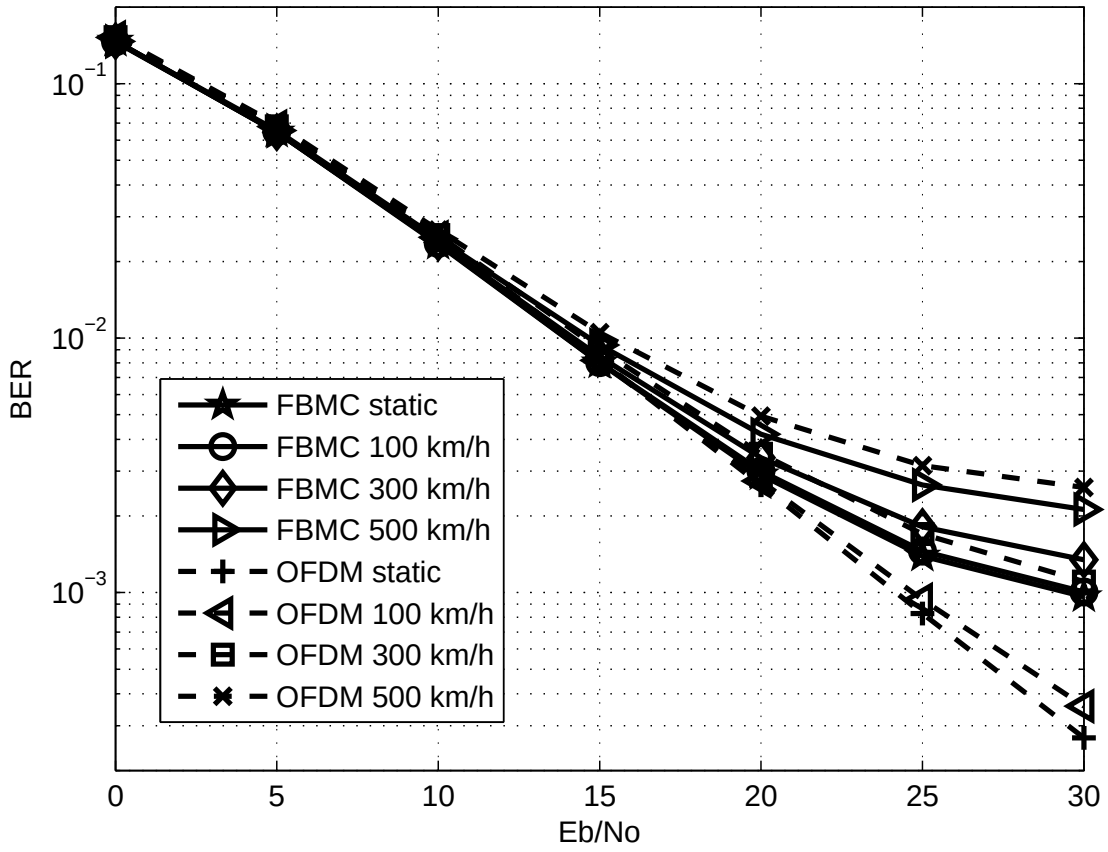

Figure 7: BER of 2-PAM (FBMC) and 4-QAM (OFDM) versus Eb/No over EVA channel.

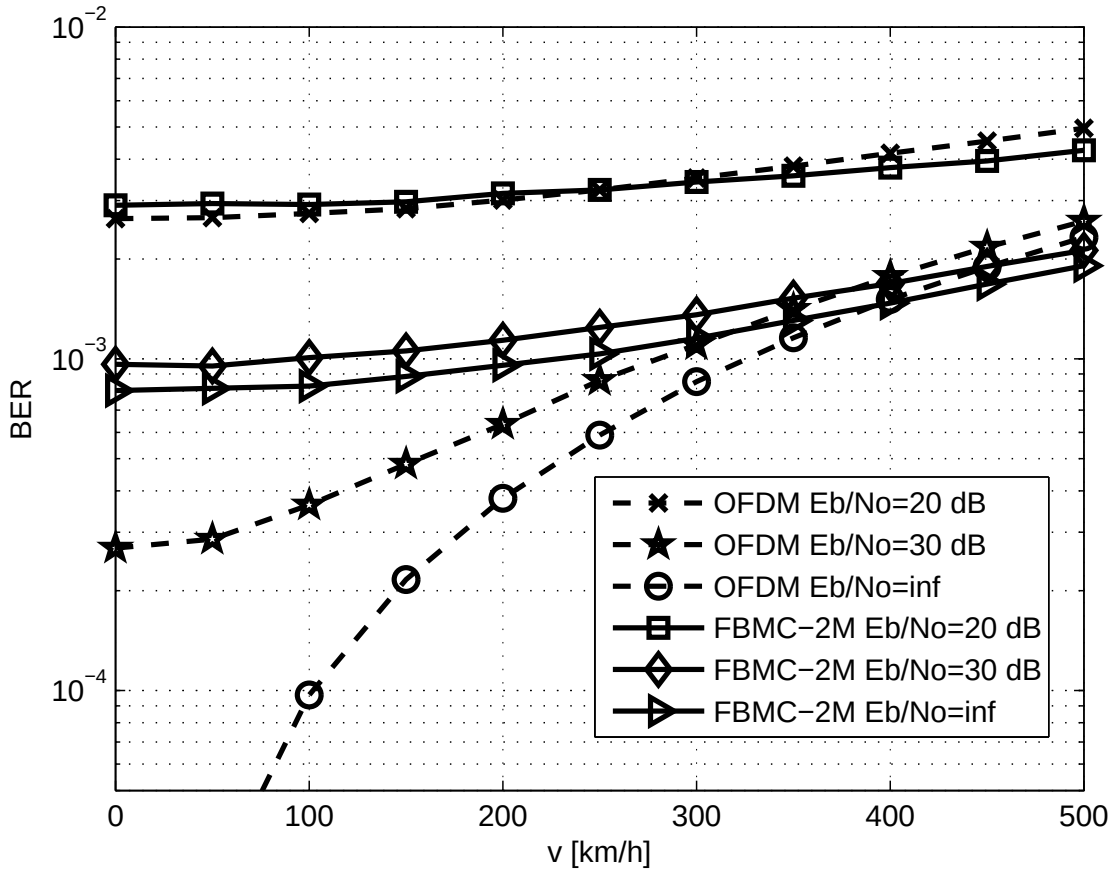

Figure 8: BER of 2-PAM (FBMC) and 4-QAM (OFDM) versus moving speed [km/h] over EVA channel.

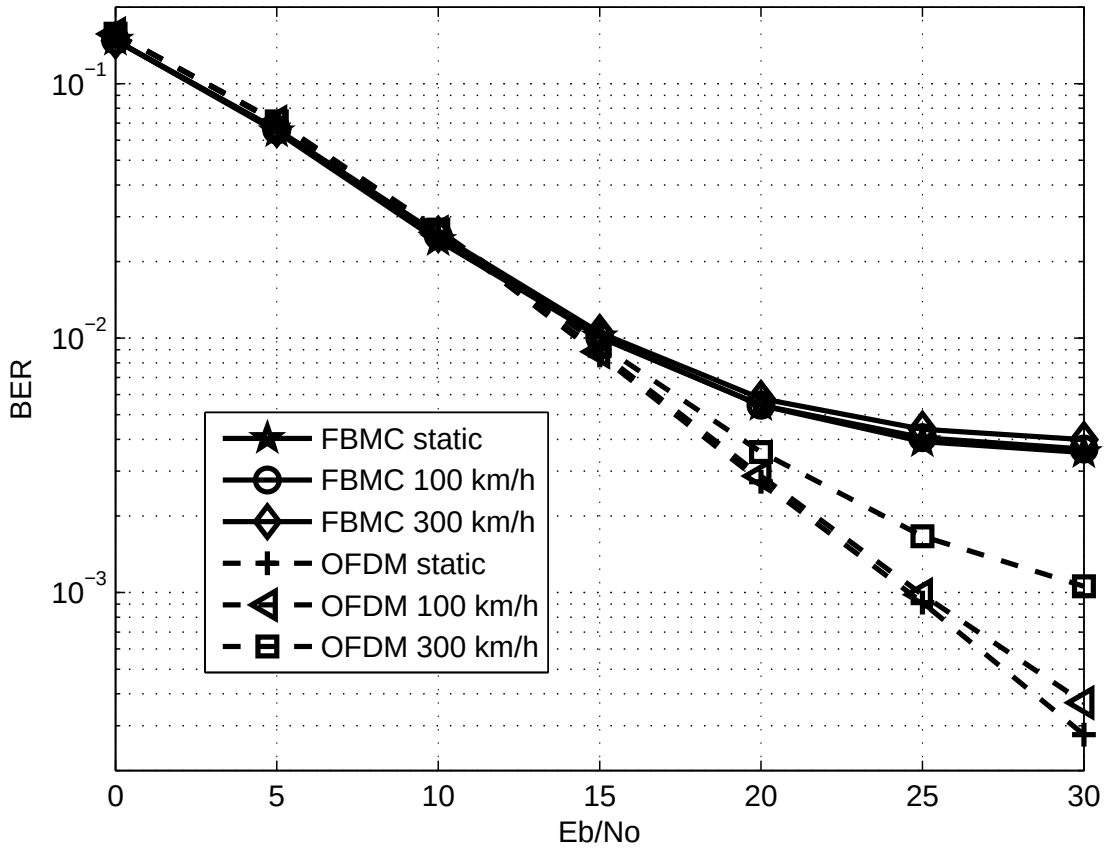

Figure 9: BER of 2-PAM (FBMC) and 4-QAM (OFDM) versus Eb/No over ETU channel.

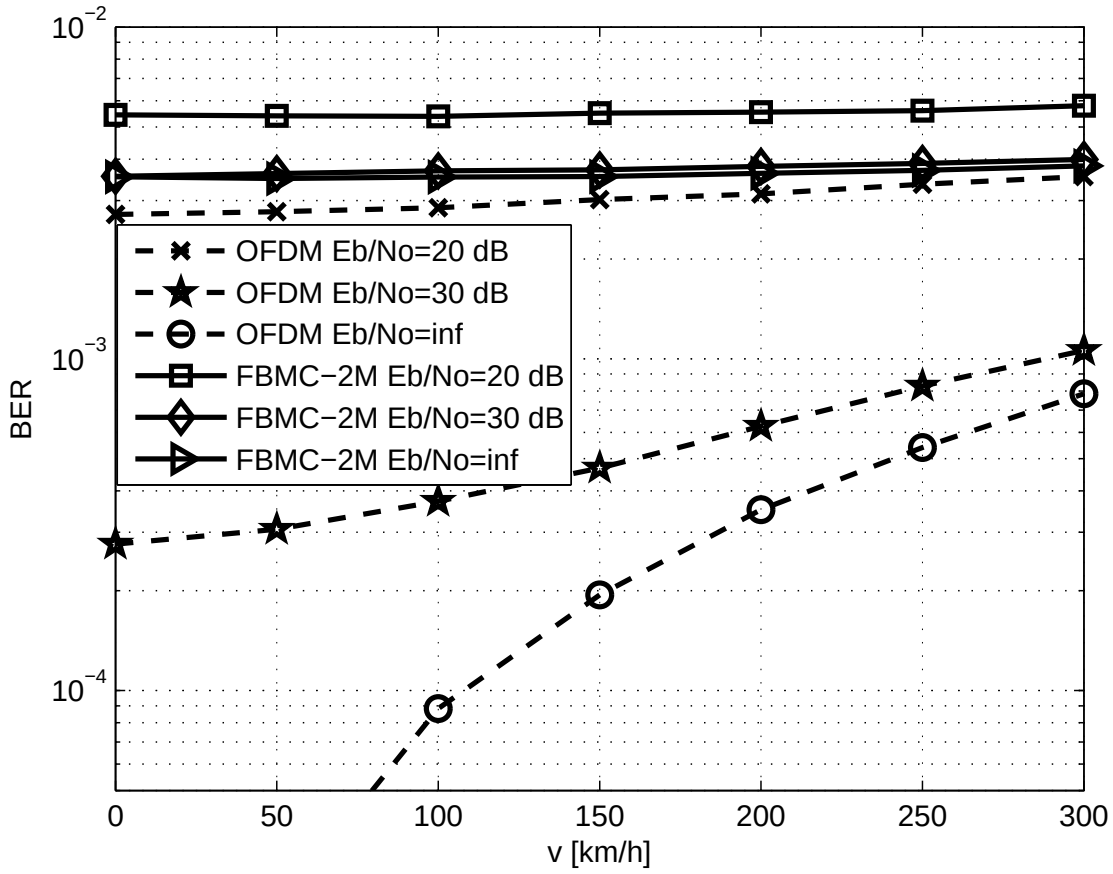

Figure 10: BER of 2-PAM (FBMC) and 4-QAM (OFDM) versus moving speed [km/h] over ETU channel.

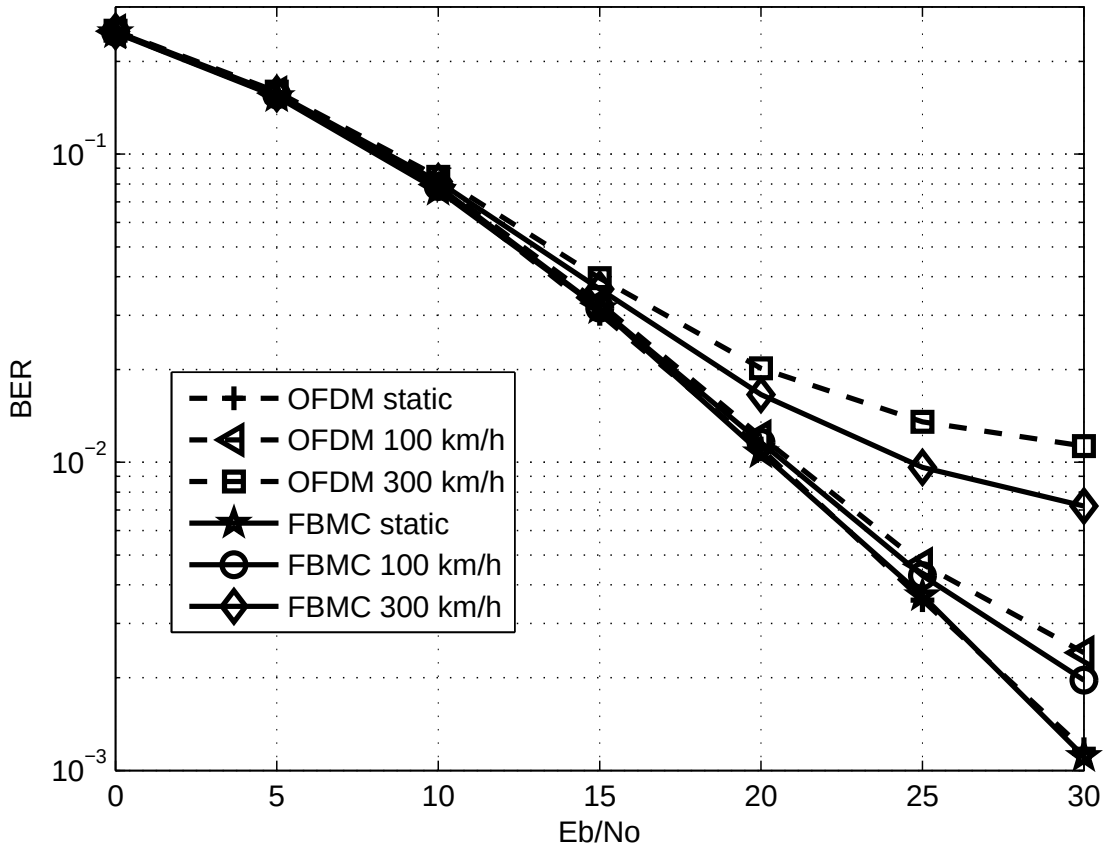

Figure 11: BER of 8-PAM (FBMC) and 64-QAM (OFDM) versus Eb/No over EPA channel.

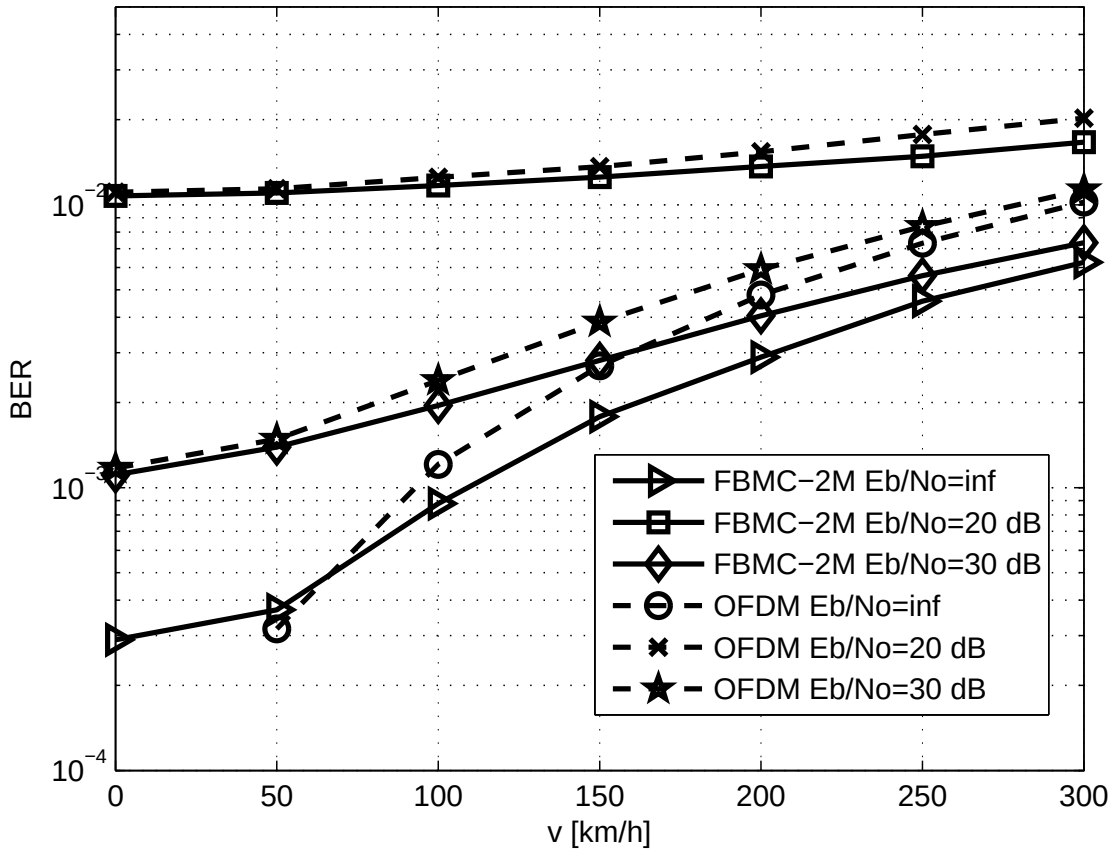

Figure 12: BER of 8-PAM (FBMC) and 64-QAM (OFDM) versus moving speed [km/h] over EPA channel.

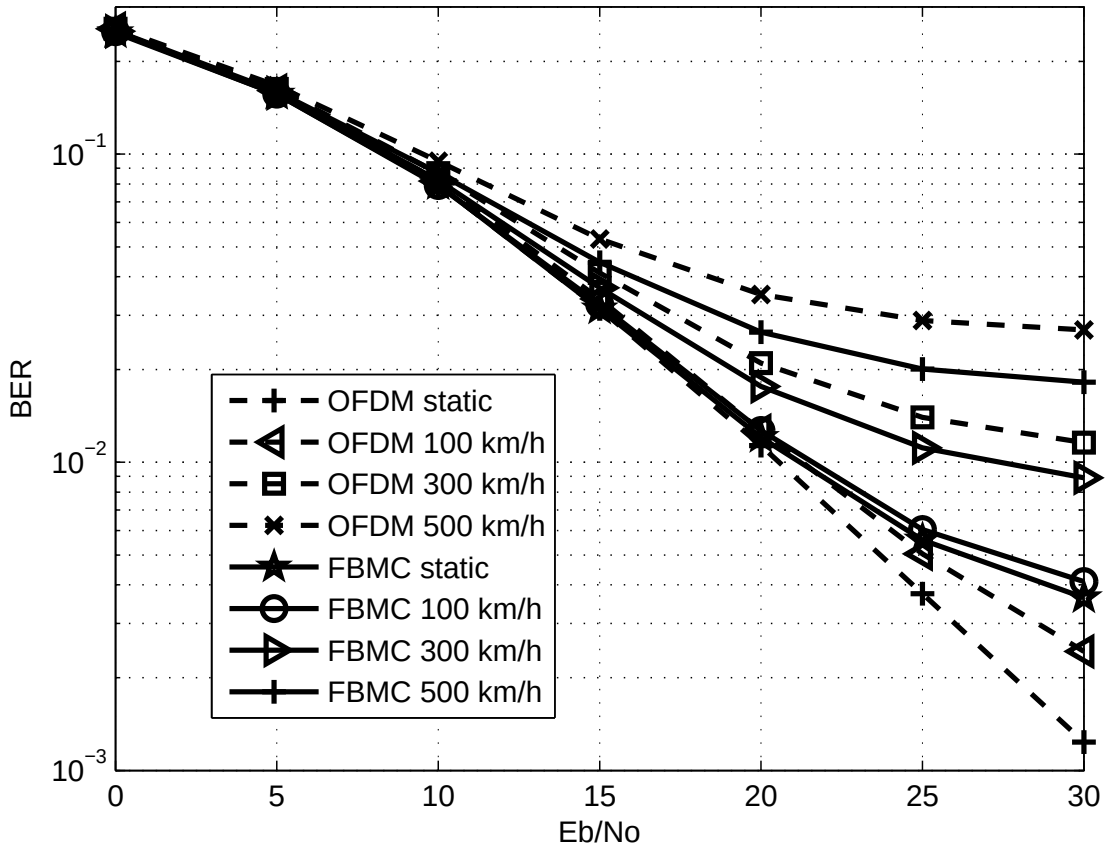

Figure 13: BER of 8-PAM (FBMC) and 64-QAM (OFDM) versus Eb/No over EVA channel.

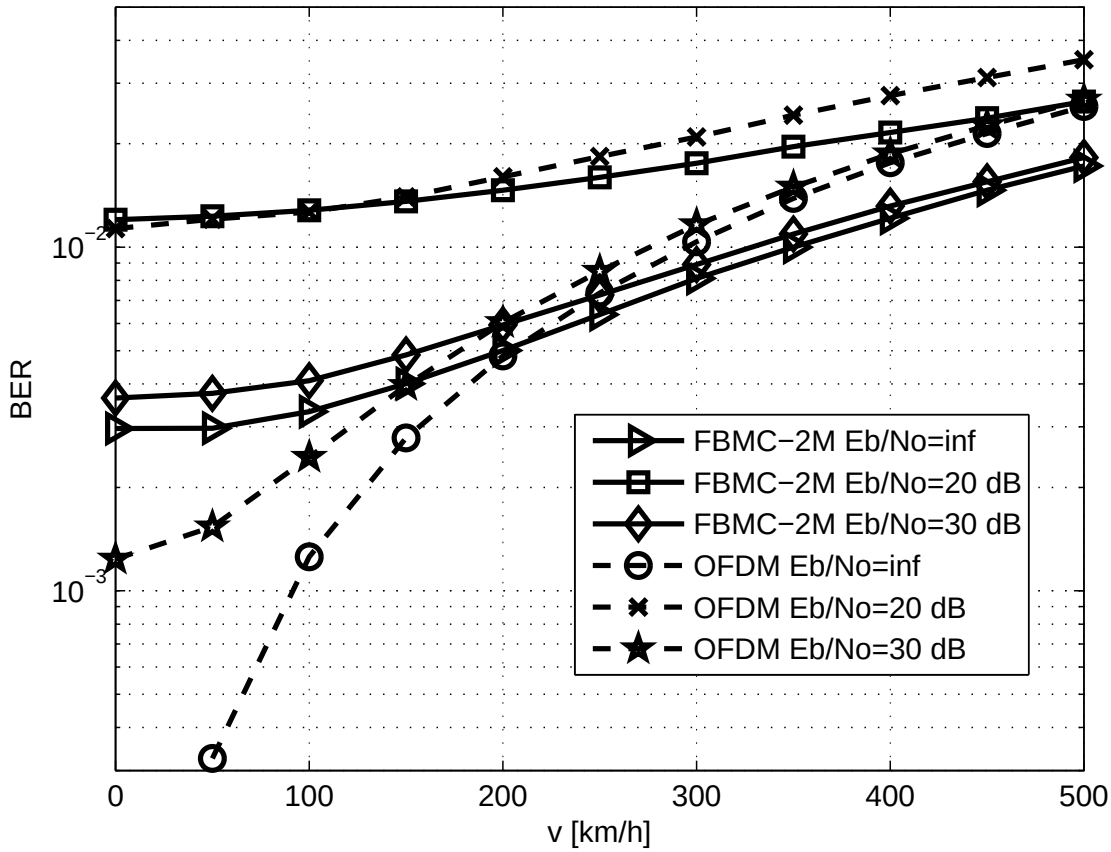

Figure 14: BER of 8-PAM (FBMC) and 64-QAM (OFDM) versus moving speed [km/h] over EVA channel.

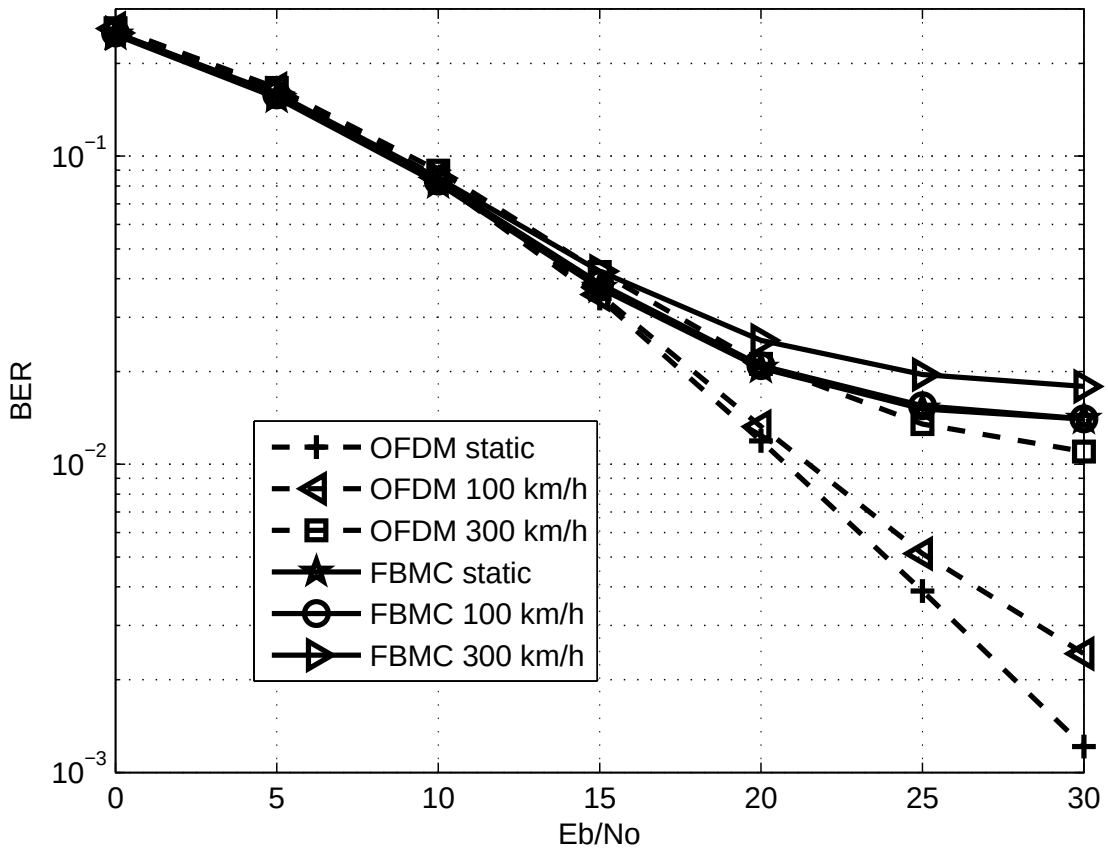

Figure 15: BER of 8-PAM (FBMC) and 64-QAM (OFDM) versus Eb/No over ETU channel.

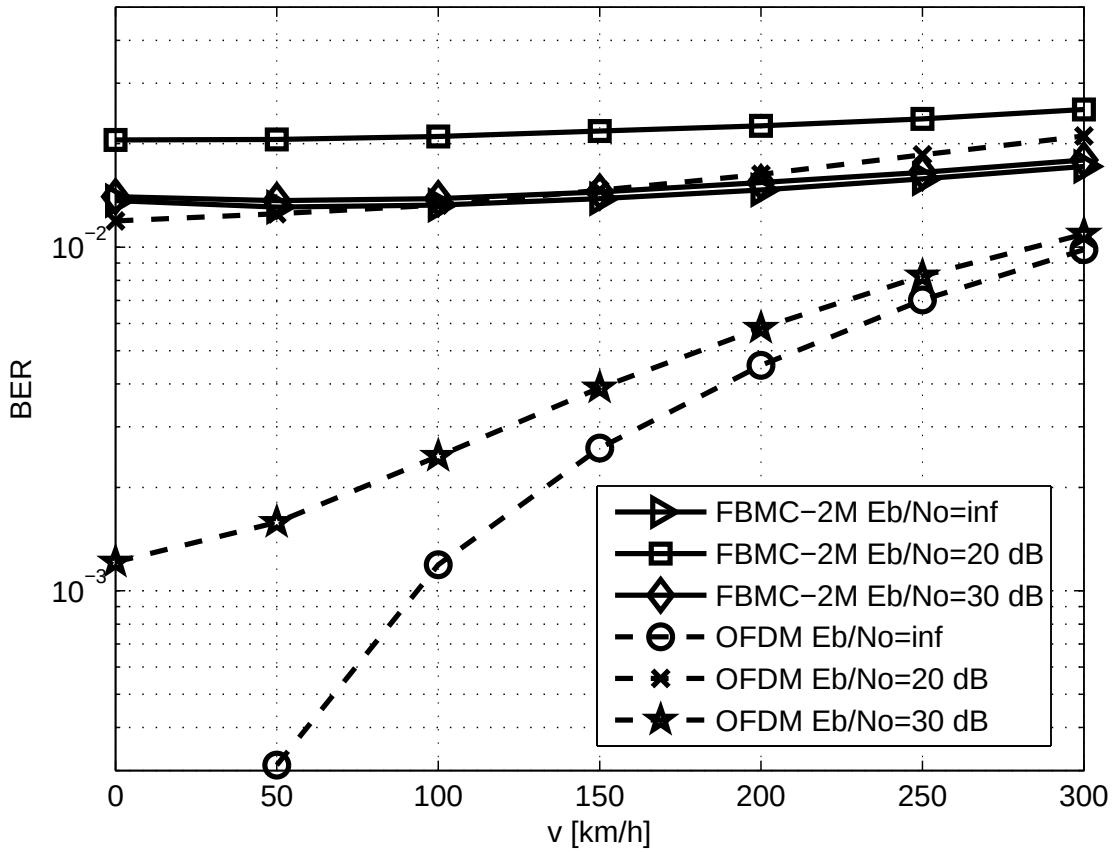

Figure 16: BER of 8-PAM (FBMC) and 64-QAM (OFDM) versus moving speed [km/h] over ETU channel.

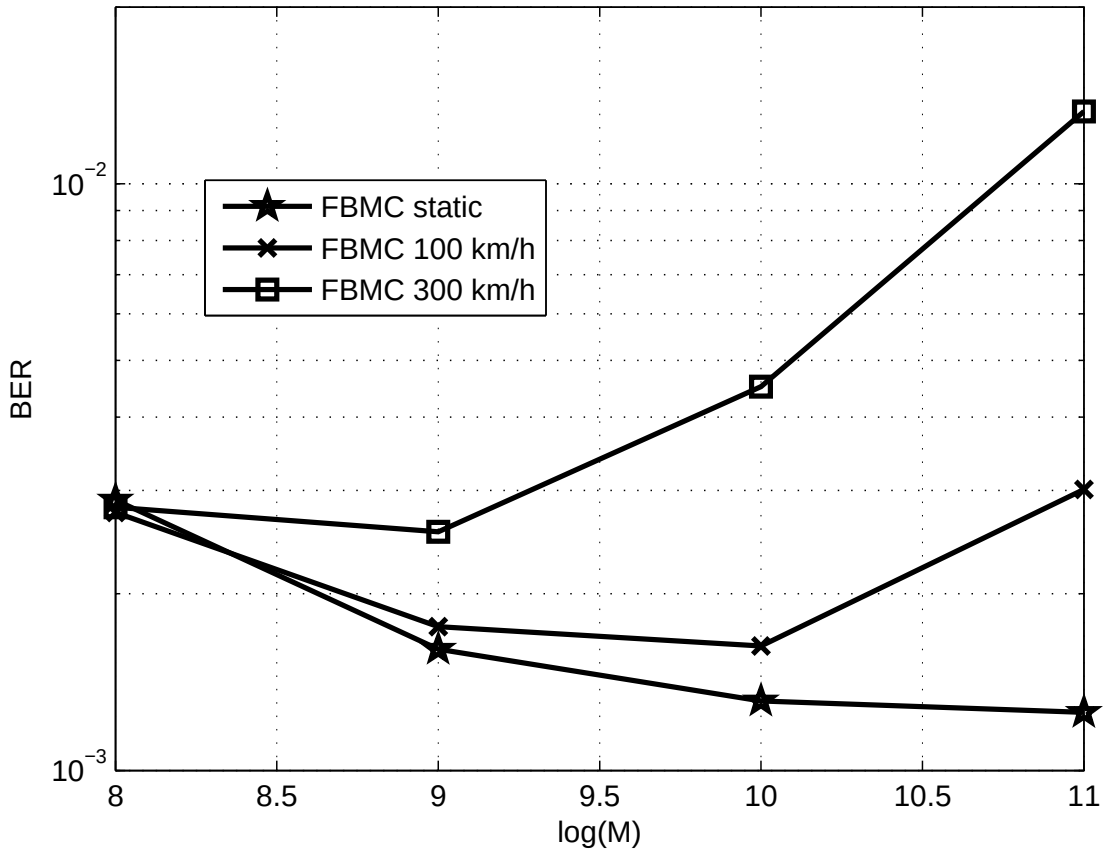

Figure 17: BER of 8-PAM (FBMC) and 64-QAM (OFDM) versus log (M) for FBMC-PAM system at Eb/No= 30 dB over EPA channel.

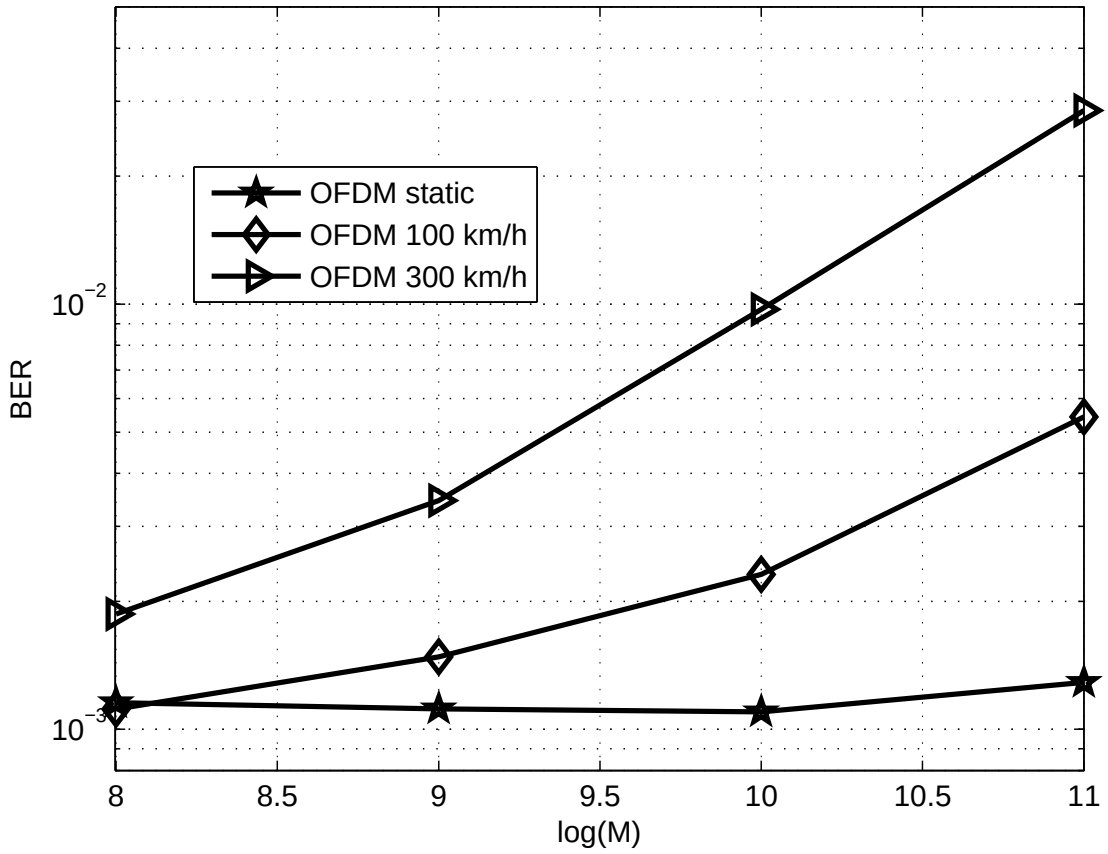

Figure 18: BER of 8-PAM (FBMC) and 64-QAM (OFDM) versus log (M) for OFDM system at Eb/No= 30 dB over EPA channel.